Crash test for the Copenhagen problem

Jan Nagler
Institut für Theoretische Physik, Otto-Hahn-Allee, Universität Bremen, 28334 Bremen, Germany
(Received 19 January 2004; published 17 June 2004)

The Copenhagen problem is a simple model in celestial mechanics. It serves to investigate the behavior of a small body under the gravitational influence of two equally heavy primary bodies. We present a partition of orbits into classes of various kinds of regular motion, chaotic motion, escape and crash. Collisions of the small body onto one of the primaries turn out to be unexpectedly frequent, and their probability displays a scale-free dependence on the size of the primaries. The analysis reveals a high degree of complexity so that long term prediction may become a formidable task. Moreover, we link the results to chaotic scattering theory and the theory of *leaking* Hamiltonian systems.

DOI: 10.1103/PhysRevE.69.066218 PACS number(s): 05.45.Ac, 05.45.Pq, 47.52.+j

I. INTRODUCTION

The restricted three-body problem (RTBP) was first considered by Euler (1772) and Jacobi (1836). Later, from 1910 to 1925, the Copenhagen group around Strömgren investigated numerically the case of equal main masses of the RTBP. Hence, this problem is called a Copenhagen problem. Despite the assumption that the third mass (the test body) does not affect the primaries the problem is nonintegrable. Due to its simplicity and cosmological relevance this problem triggered extensive numerical investigations until today; we mention only the works of Szebehely [1] and Hénon [2–5]. The RTBP, though much simpler than the general three-body problem, can still serve as a paradigm for classical chaos, see, e.g., Richter [6]. A big part of the work around the three-body problem deals with finding, describing and classifying periodic orbits. But the applications are widespread and cover classical deterministic chaos [6], semiclassical quantization, quantum mechanics, chemical [7,8] and astrophysical problems [9–12]. From diverse astrophysical viewpoints there are many recent works; the RTBP serves as a model system to investigate the stability of (extra)solar (sub)systems [13,14], (chaos assisted) asteroid capture [15], and the dynamics of two massive black holes orbited by a sun [16].

II. THE MODEL

We consider the (planar circular) restricted three-body problem for the Copenhagen case. Two equal masses move on a circle with Kepler frequency [25] about their common center of gravity assumed to be fixed (see left in Fig. 1). In the inertial system the RTBP has a time dependent potential $V_\mu(x,y,t)=-\mu/r_1(t)-(1-\mu)/r_2(t)$ where $\mu=m_1/(m_1+m_2)$, and $r_1(t)$, $r_2(t)$ are the distances to the respective primaries. The time dependence of the potential is usually eliminated using a corotating frame wherein the primaries rest. Then, the test body moves in the (x,y)-plane with Jacobi's potential $V_J=-\mu/r_1-(1-\mu)/r_2-\frac{1}{2}(x^2+y^2)$ where $r_{1,2}=(x\pm 1/2)^2+y^2$. The quadratic term results from the centrifugal force $F_{\text{cen}}=(x,y)$, whereas the Coriolis force $F_{\text{Cor}}=2(\dot{y},-\dot{x})$ gives no contribution to the potential. The *energy* [26] E of this system is conserved and (up to the factor -2) has been known historically as Jacobi's integral $C=-2E, E=\frac{1}{2}(\dot{x}^2+\dot{y}^2)+V_J$. It is widely believed that E is the only (independent) integral of this system [17]. The scaled equations of motion for the test body in the corotating frame for the Copenhagen case $\mu=1/2$ are

$$\ddot{x} = 2\dot{y} + x - \frac{x+1/2}{2{r_1}^3} - \frac{x-1/2}{2{r_2}^3},$$

$$\ddot{y} = -2\dot{x} + y - \frac{y}{2{r_1}^3} - \frac{y}{2{r_2}^3}, \tag{1}$$

wherein the radius variables are no longer explicitly time dependent. The equations of motion (1) are invariant under the symmetry operation $\Sigma:(x,y,t)\to(x,-y,-t)$. This holds for the general case $\mu\neq 1/2$. A special symmetry for the Copenhagen case is $\Sigma':(x,y,t)\to(-x,-y,t)$. These are the only known (independent) symmetries of the equations of motion (1).

III. ORBIT TYPE DIAGRAMS

The motion is restricted to 3-dimensional surfaces $E=$const in phase space. The position and extent of chaos is studied in terms of Poincaré sections (complete in the sense of Dullin *et al.* [18]). With polar coordinates (r,ϕ) in the center of mass system (COM) the condition $\dot{r}=0$ defines a 2-dimensional surface of section in the surface $E=$const, with two disjoint parts $\dot{\phi}<0$ and $\dot{\phi}>0$. Each of these two parts has a unique projection onto the (x,y)-plane. Figure 3 displays these projections for $\dot{\phi}<0$, at three different energy levels.

In contrast to common representations of Poincaré sections where the color codes indicate single orbits, here *each* pixel is given a color according to the orbit *type*. We call these diagrams *orbit type diagrams* (OTD). Roughly speaking, we classify the orbit types into bounded motion of a few kinds, unbounded motion and collision orbits.

Bounded motion: Generally, for nonintegrable systems with configuration space extending to infinity it is nontrivial

 ©2004 The American Physical Society

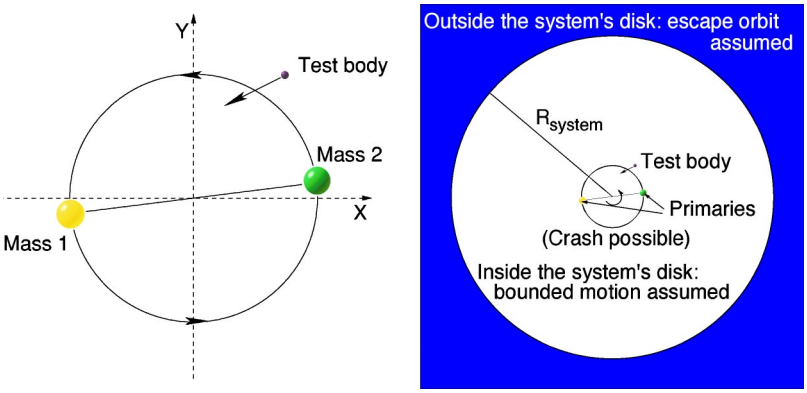

FIG. 1. Left: A schematic picture of the restricted three-body problem with equal main masses, i.e., the Copenhagen problem. Right: A schematic picture of orbit type diagrams. We call the motion bounded if the test body stays confined for a given time (t_{timeout}) inside the system's disk with radius R_{system}. If the test body leaves the disk the integration is aborted and the motion is called unbounded (escape orbit). If during the integration a crash with one of the main masses occurs we call the corresponding trajectory a crash orbit.

to prove the boundedness of motion for specific initial conditions. Here, we give a practical definition of bounded motion: We call a motion bounded if the test body stays confined for the time t_{timeout} inside a disk with center at the COM-origin and radius R_{system}. The higher the values of t_{timeout} and R_{system}, the more plausible the numerical statement *bounded motion* becomes. In the limit $t_{\text{timeout}} \to \infty$ this definition becomes the precise description of boundedness in a finite disk of radius R_{system}. Unfortunately, the higher the values of these two parameters, the longer the numerical calculation lasts. In this paper, we choose $t_{\text{timeout}}=10000$ and $R_{\text{system}}=10$. A lower value of t_{timeout} smoothens the fractal border of bounded regions [19]. We use a symbolic orbit classification for bounded motion which is suitable for an automatic identification of the orbit types. The new classification differs from the standard scheme of Strömgren, Hénon *et al.* (see, e.g., Hagihara [20] for a detailed discussion). The emphasis is on the distinction between regular motion (including small scale chaos) on the one side and strongly chaotic motion (not hindered by KAM orbits [6]) on the other. Our classification is based on an automatic detection of x axis passages of the test body. Two subsequent x axis passages are used to define a *half rotation* with respect to the fixed positions of the main masses. We label a half rotation counterclockwise around one (of the two) centers by "L," a half rotation clockwise by "R" and effectively no rotation is labeled by zero "0." For example, a quasiperiodic clockwise orbit *solely* around the first center is described by the two symbol sequences (RRR..;000…) (cf. class 1*b* in Fig. 2) where the left slot of the bracket refers to revolutions around primary 1; the right to those around primary 2. In Fig. 2 example orbits for twelve classes that we termed 1a–4 are shown. A precise description of the classes has been given earlier [19].

Unbounded motion (escape orbits): If the test body leaves the central disk with radius R_{system} at a time $t_{\text{escape}} < t_{\text{timeout}}$, we *say* that the test body has left the *system* and stop the integration. These points in the OTDs are colored from dark blue (grey) (a small value of t_{escape}) to light blue (grey) (a high value of t_{escape}). Note that the Kepler problem exhibits ellipses for all starting positions in the configuration space (x,y) for some energy level. Thus, our definition would be inappropriate for orbits that never enter the *inner* region, say, $r \lesssim 1$, and are only slightly disturbed Kepler ellipses. But in this paper, we focus our attention on the dynamics of the motion in the inner region. Moreover, thinking of a real solar system with more disturbing bodies, the definition is physically motivated.

Collision: A collision with the first primary body of radius R_{mass} occurs when the test body intersects the border of the disk around $(-\frac{1}{2},0)$ with radius R_{mass}. These points in the OTDs are colored white. A collision with the second primary body [at $(+\frac{1}{2},0)$] is defined analogously but colored red (grey). See the right part of Fig. 1 for a schematic picture of OTDs.

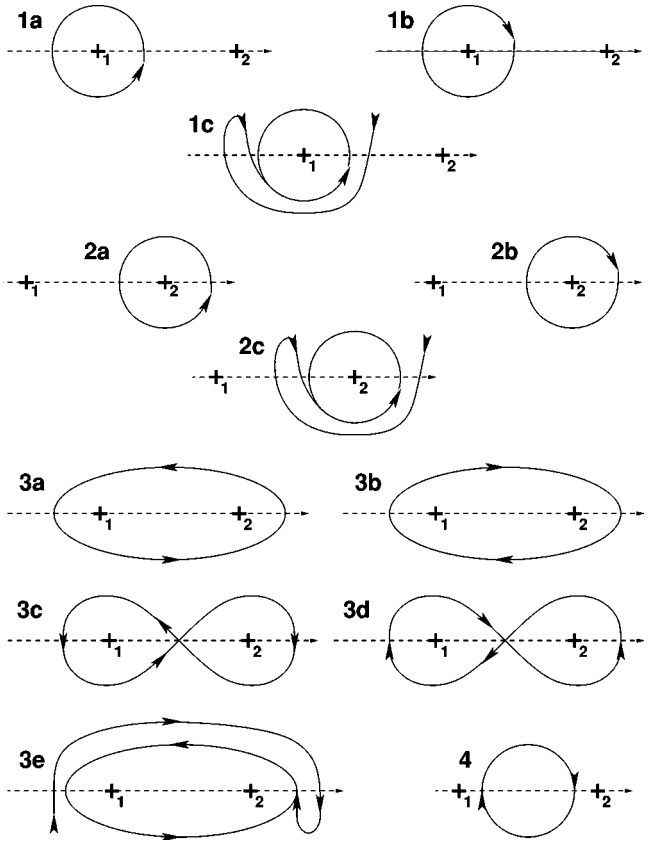

FIG. 2. Symbol sequences for the orbit examples: Class 1*a*:(LLL…;000…), 1*b*:(RRR…;000…), 1*c*:(R0LLL…;000…). Class 2*a*:(000…;LLL…), 2*b*:(000…;RRR), 2*c*:(000…;R0LLL…). Class 3*a*:(LLL…;LLL…), 3*b*:(RRR…;RRR…), 3*c*:(L00LL00L…;0RR00RR0…), 3*d*:(R00RR00R…;0LL00LL0…), 3*e*:(R0LLL…;R0LLL). Class 4:(000…;000…). Note that the orbits need not be periodic to have the same symbol sequences.

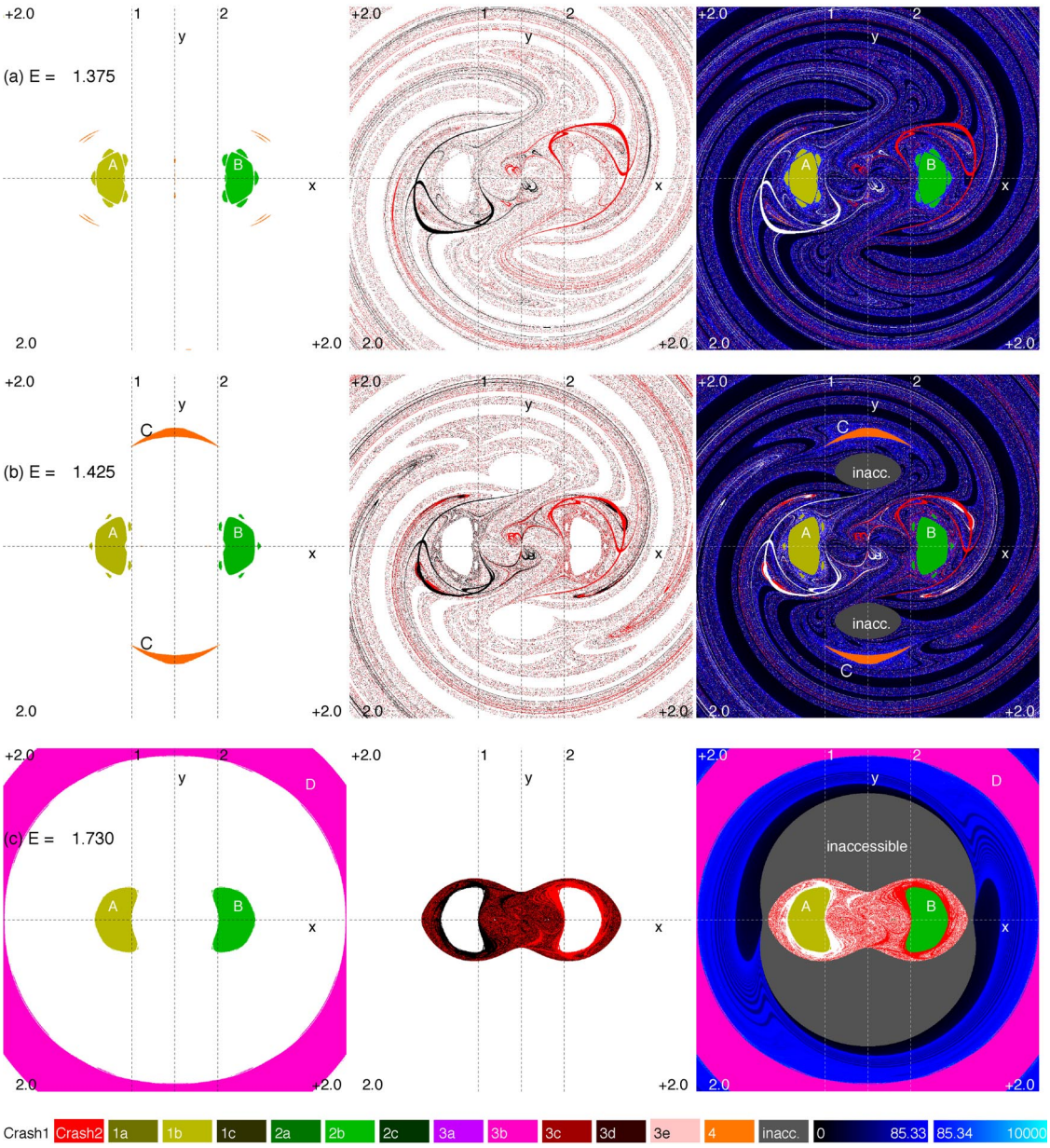

FIG. 3. (color online) Regions of bounded motion (left column), crash orbits (middle column) and together with regions of escape orbits (right column) for three different energy levels. The (x,y)-plane in a corotating frame of reference for the Copenhagen problem is shown. The color of a point represents the orbit type of a test body which has been launched with the pericenter position at (x,y) for the energy level E (see the orbit class legend below). Top (a) Decomposition of the OTD at $E=-1.375$. Bounded motion is indicated by the colors (grey scales) of classes 1a–4. White (red/black) points indicate a collision with mass 1 (2). Escape orbits are colored black ($t_{\text{escape}}=0$) to blue (grey) ($t_{\text{escape}}=10000$). Middle row (b) Decomposition for same conditions but at the energy level $E=-1.425\,781\,25$. Bottom (c) Decomposition for $E=-1.730\,468\,75$. Initial condition: $\dot{r}=0, \dot{\phi}<0$. Radii of the primaries (not shown): $R_{\text{mass}}=8.97\times10^{-5}$.

IV. THE (x,y)-PLANE

The pictures to the right in Fig. 3 represent OTDs with respect to the center of mass (COM) at the origin $(0,0)$ for different energy levels. The (x,y)-plane (in the corotating frame of reference) is displayed. The pictures to the left in Fig. 3 display the regions of bounded motion in the OTDs. In the middle column the crash basins for the three energy levels are shown. The diagrams in Fig. 3 exhibit the symmetry Σ' (because it is also respected by the section condition).

Figure 3(a) shows the OTD decomposition for the fixed energy $E=-1.375$. There is a main region A of bounded motion around mass 1 which consists of a central region, surrounded by five small and one tiny islands. Each region of regular motion has a resonance, i.e., a periodic orbit at its center. The regions in white (black) represent the start positions where the test body eventually crashes with mass 1. These *crash basins* wind out as spirals in the outer regions of the diagram, due to the rotating primaries. But there appear crash basins also in the immediate neighborhood of the

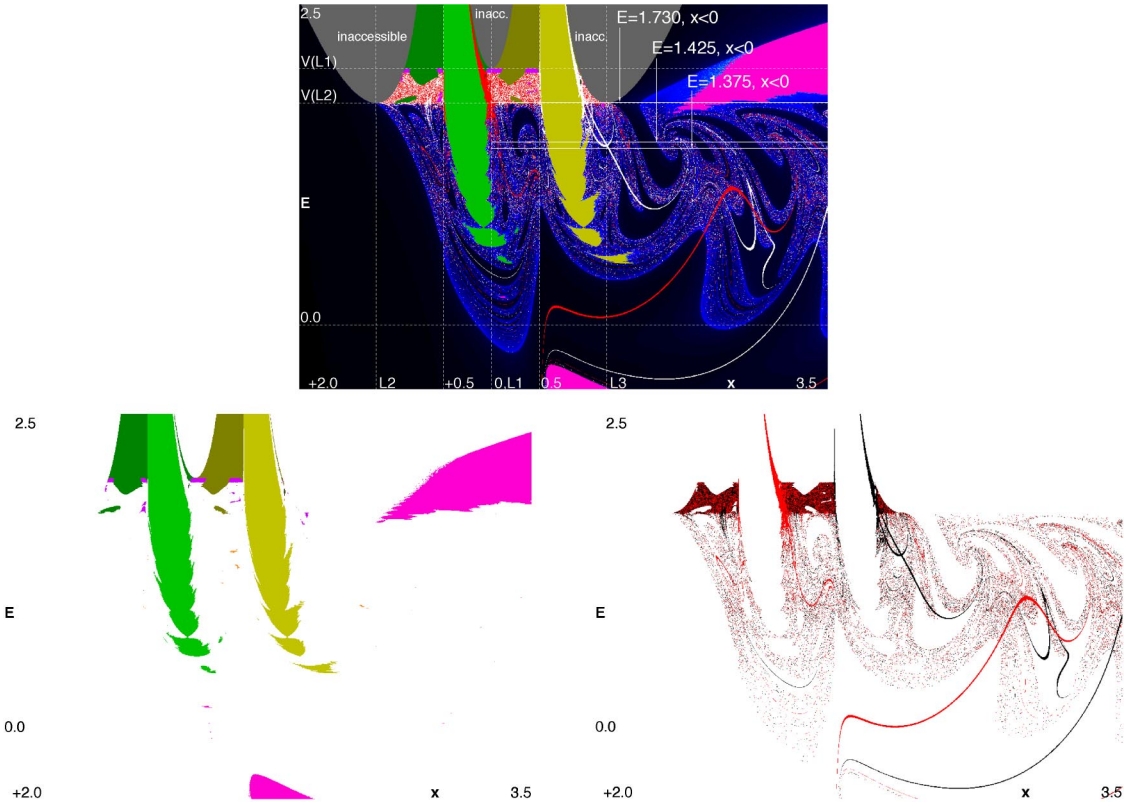

FIG. 4. (color online) Top: Orbit type diagram for the (x,E)-plane. Poincaré section: $y=\dot{x}=0,\dot{y}>0$. Radii of the primaries: $R_{\text{mass}}=8.97\times10^{-5}$. The symbols $L_{1,2,3}$ represent the x-positions of the corresponding Lagrange points and $V_J(L_{1,2})$ are the potential values of the first two. Additionally, the three energy levels of Fig. 3 are highlighted. See Fig. 3 for a color legend. Bottom: Bounded motion of the OTD (to the left) and crash basins (to the right). Crash onto primary 1: black; crash onto primary 2: red (grey).

COM. Note that the primary body disks are several orders of magnitude smaller in area than the total size of crash basins. In this representative Poincaré section, the phase space is a close mix of crash basins, regions of bounded motion and escape basins. The fixed energy level $E=-1.375$ represents the so-called Trojanic energy corresponding to the maxima of Jacobi's potential. Thus, the test body has access to the full (x,y)-plane.

In Fig. 3(b) the corresponding (x,y)-plane for $E=-1.425\,781\,25$ is shown. There are inaccessible regions (grey) in the plane because the energy is smaller than the Trojanic energy. The orange colored islands (C) belong to a well-known orbit of type 4.

Fig. 3(c) displays the (x,y)-planes for the energy $E=-1.730\,468\,75$. Here, the inaccessible area (grey) separates two regions. In the outer region there is a ring of bounded motion (rose colored; D) which separates regions of escape orbits. In the inner zone the test body is confined. The regions A and B indicate stable motion around the individual primaries. These regions are surrounded by a chaotic mix of areas of crash orbits with respect to the first and the second primary body.

Interestingly, the OTDs in Fig. 3 possess both, smooth (nonfractal) and fractal regions of the boundaries which separate the regions of escape orbits and the crash basins. In the context of *leaking* Hamiltonian systems the boundaries are classified to be of type II [21–23]. Here, the leakages are defined by the crash conditions and the escape condition resulting in three *exit modes*. As a consequence, the boundaries make it difficult to predict whether the test particle (e.g., an asteroid) hits a primary body or leaves the (solar) system. The OTDs differ only slightly from those obtained using a suitable defined escape velocity condition, e.g., $\dot{r}>[2/(r-1)]^{1/2}$, rather than the escape condition $r>R_{\text{system}}$ used here. Thus, the occurrence of *escape basins* [colored solid dark blue (grey)] is not an artifact of the arbitrarily chosen escape condition.

V. THE (x,E)-PLANE

The diagrams in the (x,y)-plane provide information on the phase space mixing for only a fixed energy. Hénon considered a plane which provides information about regions of stability and regions of escape orbits using the section $y=\dot{x}=0,\dot{y}>0$, i.e., the test body starts on the x-axis, parallel to the y-axis and in the positive y-direction. Thus, in contrast to the section discussed before, only orbits with pericenters on the x-axis are included. But then the energy E is used as an ordinate. Figure 4 shows an OTD decomposition for the (x,E)-plane. The corresponding energy levels of the (x,y)-diagrams in Fig. 3 are also shown. Note that the energy $E=-C/2$ increases downwards and x decreases from the left to the right. A comparison of the stability diagram in [3] (not shown) and Fig. 4 highlights the impressive accuracy of

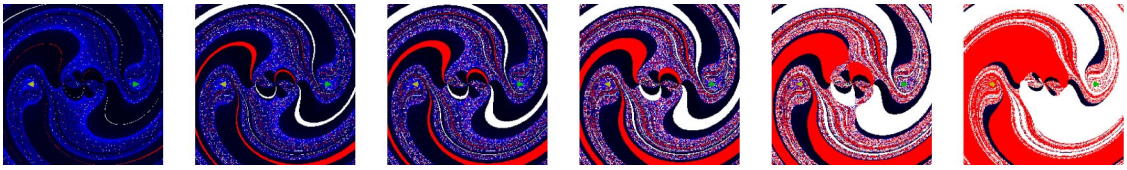

FIG. 5. (color online) An extension of the crash basins [white and red (grey)] for different primary body raddii. Orbit type diagrams for the (x,y)-plane at the energy level $E=-0.5$ for the Copenhagen problem are shown. The surface of section conditions: $\dot{r}=0, \dot{\phi}<0$. Range: $x,y=-2.0\ldots2.0$. Radii of the primaries (from left to right): $R_{M_1}=R_{M_2}$: $10^{-5}, 10^{-3.5}, 10^{-2.5}, 10^{-2}, 10^{-1.5}, 10^{-1}$. See Fig. 3 for a color legend.

Hénons work of the sixties where the speed of computation was several orders of magnitude lower than today and terms like deterministic chaos or fractal boundaries were only beginning to emerge.

The boundaries between bounded and unbounded motion are now seen to be more jagged than shown in the stability diagram. Moreover, we found in the blow-ups of the diagram many tiny islands of stability (and resonances in their centers). From chaos theory we expect indeed an infinite number of islands of (stable) quasiperiodic (or small scale chaotic) motion. The region between the potential values of the first two Lagrange points $V(L_{1,2})$ shows many tiny islands of regular motion plus a chaotic mix of areas of crash orbits (cf. OTD for $E=-1.73$ in Fig. 3).

VI. SCALING LAW FOR THE CRASH BASINS

So far the radii of the primaries were arbitrarily assumed to be fixed at $R_{M_{1,2}}=8.97\times10^{-5}$. Figure 5 displays OTDs for the fixed energy $E=-0.5$ with radii $R_{M_{1,2}}$ increasing from 10^{-5} to 10^{-1}. The area of crash orbits with respect to the first primary body follows a power law over several orders of magnitude: $A_{\text{crash}}\sim R^{\alpha}$ with $\alpha=0.46(2)$. Figure 6 shows the corresponding log–log plot for the energy level $E=-0.5$. Due to the nonintegrability of the RTBP it seems nontrivial to calculate exactly the power law behavior. Thus, we derive a rough approximation for $A_{\text{crash}}(R)$. First, we consider the RTBP when the test body is close to one primary body (just before a crash occurs). Second, we neglect the rotation of the primaries. Then, the situation can be (roughly) approximated by the Kepler problem. Using the relation $E=E_{\text{in}}-L$ between the energy in the inertial system E_{in} and the angular momentum L from Kepler's ellipse formula it follows that

$$E=-\frac{1}{r_a+r_p}\mp\sqrt{\frac{2r_p r_a}{r_p+r_a}}, \tag{2}$$

where r_p denotes the perihelion and r_a the aphelion distance. Solving Eq. (2) for r_a yields

$$r_a(r_p)=-r_p-\frac{E+r_p^2}{E^2-2r_p}-\frac{\sqrt{r_p^4+2Er_p^2+2r_p}}{E^2-2r_p}. \tag{3}$$

Note that $r_a>r_p>0$ implies first $E<-1/2r_p$, and second the negative root in Eq. (3). A collision occurs when the test body intersects the disk with radius R around the Kepler singularity: $r_p\leqslant R$. Thus, for $R\ll1$ the area of crash orbits can be approximated by $A_{\text{crash}}(R)\approx2\pi r_a(0)[r_a(0)-r_a(R)]$. But for $r_p\ll1$, Eq. (3) is approximated by $r_a(r_p)\approx-1/E+\sqrt{2r_p}/E^2$. Hence, we obtain a power law $A_{\text{crash}}(R)\sim R^{\beta}$ with the exponent $\beta=1/2$. The power law has been approximately confirmed by simulations of the RTBP for different values of the mass ratio μ, and for different energy levels E (from -1.375 up to 0.5).

VII. CONCLUSIONS

To conclude, the orbit type diagrams that we introduced display the phase space mixing of bounded, unbounded and crash orbits in a new kind of Poincaré section representation. The diagrams extend known behavior in the RTBP. Moreover, they provide detailed information about extent and position of the different regions and display the complex boundaries between them.

From the theory of *leaking* Hamiltonian systems [23] it follows that the boundaries, between the crash basins and the regions of escape orbits represent the *chaotic saddle* (i.e., the invariant manifolds) plus existing KAM tori better the smaller the primary disks. This links the crash basins to the foliation of the phase space. Bleher *et al.* [21] proposed the

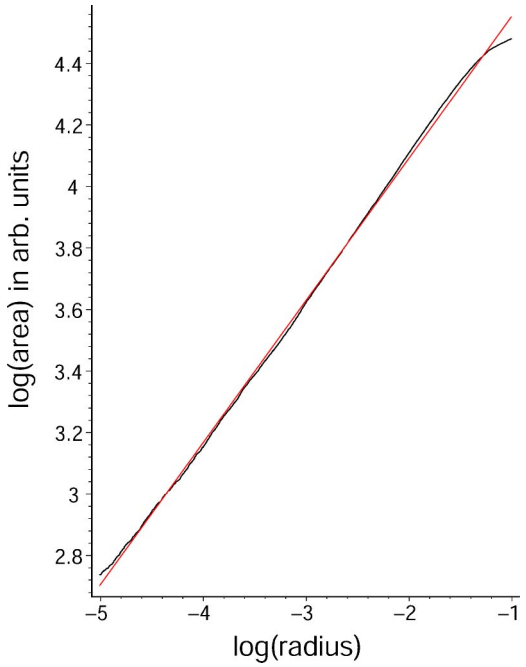

FIG. 6. (color online) Log–log plot of the crash basin size in the (x,y)-plane $(x,y=-2+2)$ at fixed energy $E=-0.5$ in arbitrary units versus the primary body radii $R=10^{-5}\ldots10^{-1}$. Black line: Numerical result. Red (grey) line: Fit curve $A_{\text{crash}}\sim R^{\alpha}$.

RTBP as an interesting application for a leaking Hamiltonian system. Here we discuss this application, resulting in the so-called type II boundaries between regions of crash and escape orbits. Moreover, the type II boundaries confirm the results of de Moura *et al.* [22]. Due to the extended primaries the model is more applicable to realistic situations of celestial body problems than the pure RTBP. The analysis reveals a high degree of complexity so that the long term prediction in comparable celestial systems may become a formidable task.

Finally, the crash basins as part of the diagrams are widely more extended than expected. The results show how comparatively small primaries affect regions of crash orbits which (to our knowledge) has not been investigated in simple celestial models as the RTBP. The size of the crash basins follows a power law that is close to the result of a calculation based on Kepler's ellipse formula.

In a companion paper [24] we investigate bifurcation schemes of periodic orbits and link the results to the underlying invariant manifolds. Furthermore, we consider the general $\mu \neq 1/2$-case of the RTBP.

ACKNOWLEDGMENTS

I warmly acknowledge P. H. Richter, T. Tél and H. R. Dullin for fruitful discussions and helpful comments.

[1] V. Szebehely, *Theory of Orbits* (Academic Press, New York, 1967).
[2] M. Hénon, Bull. Astron. **1**, 57 (1966).
[3] M. Hénon, Bull. Astron. **1**, 49 (1966).
[4] M. Hénon, *Generating Families in the Restricted Three-Body Problem* (Springer-Verlag, Berlin, 1997).
[5] M. Hénon, *Generating Families in the Restricted Three-Body Problem. II. Quantitative Study of Bifurcations* (Springer-Verlag, Berlin, 2001).
[6] P. H. Richter, Rev. Mod. Astron. **14**, 53 (2001).
[7] A. F. Brunello, T. Uzer, and D. Farrelly, Phys. Rev. A **55**, 3730 (1997).
[8] E. Lee, A. F. Brunello, and D. Farrelly, Phys. Rev. A **55**, 2203 (1997).
[9] M. A. Murison, Astron. J. **98**, 2346, 2383 (1989).
[10] T. I. Maindl and R. Dvorak, Astron. Astrophys. **290**, 335 (1994).
[11] N. Haghighipour, Mon. Not. R. Astron. Soc. **304**, 185 (1998).
[12] N. Haghighipour, Mon. Not. R. Astron. Soc. **316**, 845 (1999).
[13] J. Liebert and W. B. Hubbard, Nature (London) **400**, 316 (1999).
[14] J. J. Lissauer, Nature (London) **419**, 355 (2002).
[15] S. A. Astakhov, A. D. Burbanks, S. Wiggins, and D. Farrelly, Nature (London) **423**, 264 (2003).
[16] G. D. Quinlan, New Astron. **1**, 35 (1996).
[17] H. Poincaré, *Les Méthodes Nouvelles de la Mécanique Céleste* (Gauthier-Villars, Paris, 1892), translated by the AIP, History of Modern Physics and Astronomy, 1993, Vol. 13.
[18] H. R. Dullin and A. Wittek, J. Phys. A **28**, 7157 (1995).
[19] J. Nagler, Ph.D. thesis, Universität Bremen 2002.
[20] Y. Hagihara, *Celestial Mechanics. Vol. IV. Part 1, 2: Periodic and Quasi-Periodic Solutions* (Japan Society for the Promotion of Science, Tokyo, 1975, Vol. XV, p. 1243).
[21] S. Bleher, C. Grebogi, E. Ott, and R. Brown, Phys. Rev. A **38**, 930 (1988).
[22] A. P. S. de Moura and C. Grebogi, Phys. Rev. E **66**, 046214 (2002).
[23] J. Schneider, T. Tél, and Z. Neufeld, Phys. Rev. E **66**, 066218 (2003).
[24] J. Nagler, "Bifurcation schemes in the restricted three-body problem," in preparation.
[25] The distance between the two primaries is scaled to unity and a time unit is related to the unit angular velocity of the primaries, i.e., one rotation corresponds to 2π time units.
[26] The energy in the inertial system E_{in} is the sum of E and the angular momentum L, i.e., $E_{\mathrm{in}}=E+L$.